Study of bubbles entrapment by gas-sheared liquid film using BB-LIF technique

David B. Hann[1,*], Andrey V. Cherdantsev[2], Barry J. Azzopardi[1]
[1]Faculty of Engineering, University of Nottingham, Nottingham, UK
[2]Kutateladze Institute of Thermophysics, Novosibirsk, Russia
*corresponding author: david.hann@nottingham.ac.uk

Abstract At high enough gas and liquid flow rates, the surface of gas-sheared liquid films are covered by a complex system of waves of different scales. Disruption of ripples on top of disturbance waves by a strong gas shear leads to creation of droplets that entrained into the core of gas stream. In addition, gas may be entrapped by film surface in form of bubbles of various sizes. Measurement of the gas bubble sizes using imaging techniques have struggled due to the presence of strong optical distortions when disturbance waves are present.
In this work, the study of gas-sheared liquid film was performed in horizontal rectangular duct using high-speed brightness-based LIF technique. This technique directly measures the thickness of the liquid layer to a resolution of 0.040 mm over a 50mm by 20 mm area simultaneously at speeds of 10 kHz using a high speed camera and pulsed laser set up. Nine experiments were carried out at three liquid Reynolds numbers and three gas Reynolds numbers. These visualizations contain significant information of the physical mechanisms present and are being analysed to identify the behaviour of disturbance waves, droplet entrainment and splashing amongst others in a series of papers under development.
In this paper an automated analysis of the images to detect bubble locations and sizes is carried out and the procedure will be explained in the full paper. Bubbles embedded in the fluid are detectable as significant decreases in the thickness of the liquid film and are detectable even where there are disturbance waves.
Analysis of the BBLIF images has produced a time sequence of instantaneous bubble size distributions in situations with and without the presence of disturbance waves. It is demonstrated that there are more bubbles present in the disturbance wave because of the presence of more fluid in the disturbance waves. The number of bubbles per unit volume is shown to be consistently within error for each case over the entire analysis, but to increase with increasing Reynolds number of liquid and air.

Keywords: bubble sizes, sheared gas-liquid flows, Laser Induced Fluorescence

1 Introduction

The entrainment of gas into a liquid in sheared flow, such as annular flow in pipes, is of interest to a range of industrial areas. The entrainment of the gas can strongly influence flow characteristics, enhance chemical reactions and influence heat transfer. The droplets are created by the disruption of ripples on top of the disturbance waves by a strong gas shear **[1, 2]**. These droplets impact on the surface of the liquid and can generate bubbles. It has also been suggested **[3]** that a second mechanism of gas entrainment occurred by the breaking of the disturbance waves similar to the action of bubble entrainment in the ocean. Breaking surface waves in the ocean generate bubbles over a range of sizes. The sizes and number of the bubbles are dependent on the turbulent fragmentation. Larger bubbles are less probable because of fragmentation due to turbulent shear stress **[6]**. Below a critical bubble Webber number of around 3-4.7, which is related to the Hinze scale of the turbulence, the bubbles are more likely not to be sheared and are sustained by surface tension effects.

This study is part of a series that is using a new technique; Brightness-Based Laser induced Fluorescence, to investigate multi-phase sheared flow **[5]**. Previous work using this technique has determined that there are two mechanisms for droplet generation linked to the interaction of ripple and disturbance waves; ligament formation and bag-breakup **[6]**. The droplets produced by these mechanisms have been shown to impact the base film with two possible outcomes; crater impact or furrow impact depending on the impact angle **[7]**. It has been identified that furrow impacts most often occur on the base film and these impacts can generate a series of bubbles. **Figure 2** shows an example of the height of the film before and after a furrow impact. From this it can be seen that there are a large number of bubbles of the order of 80-200 microns in size created by the impact. It has further been noted that many of these bubbles disappear after a short period of time and must be related to surface bubbles **[7]**. This specific analysis of individual impacts is enhanced in this paper to look globally at the entrainment rate of gas. A comparison will be made between images where

there are disturbance waves, to those where there are no disturbance waves, to identify if there are differences in the bubble size distribution between the two cases.

2 Methodology

The experiments were carried out in the shearing flow rig at Nottingham University. Figure 1 shows the schematic of the experiment. The duct was rectangular in profile with a width of 161mm, a height of 25 mm. The measurements were taken 1.2 m downstream from the inlet. The experiments were carried out at three air velocities and three liquid volume flow rates to generate 9 cases. Three segments of 0.2 seconds were taken for each of the 9 cases. The flow parameters are shown in Table **1** and resulted in strong disturbance waves being generated in the rig.

The BB-LIF technique is relatively simple. The fluid (in this case water) was doped with low levels of a fluorescent dye (Rhodamine 6G) which is then illuminated by a pulse laser at rates of 10 kHz. The absorbed light is re-emitted at a different wavelength and this light is filtered and then captured by a high speed camera located below the duct. The resolution of the images was 0.04 mm/pixel and area illuminated by the laser is 20mm x51 mm. For each case three time segments of 0.2 second were taken and then simply concatenated into a single time sequence. An example of a segment of one of these images is shown in Figure 2.

Table 1: A summary of the flow rates used for the 9 cases studied in this work.

Flow parameter:	
Superficial Gas velocities	25, 30, 35 m/s
Liquid Reynolds numbers $R = (q/\nu)$	220, 360, 520

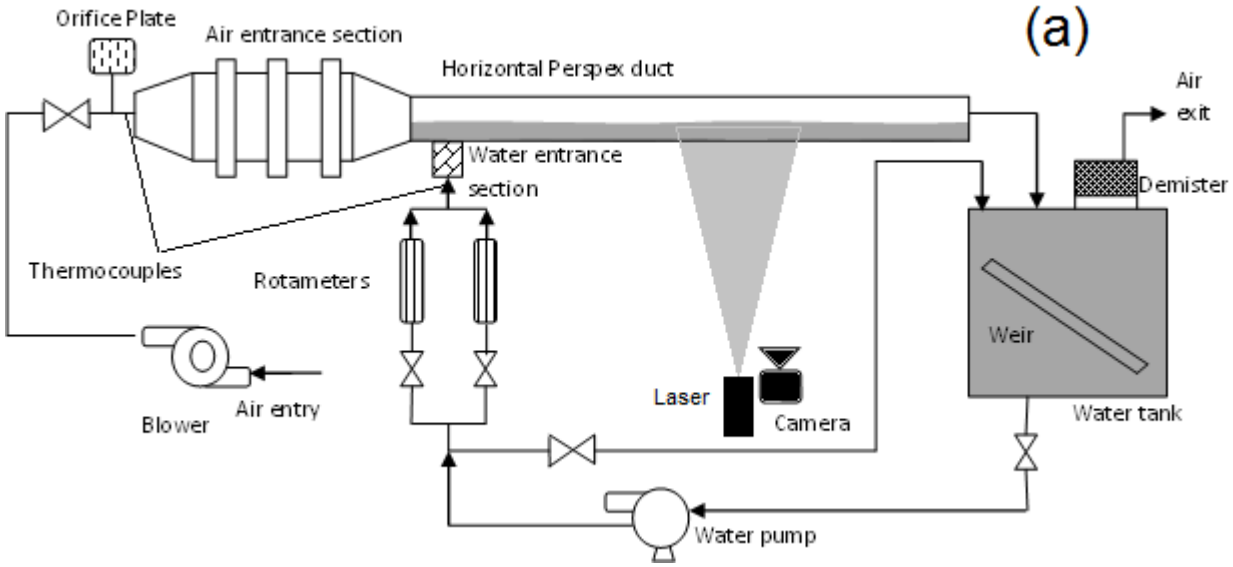

Figure 1: A schematic diagram of the shearing rig and the BB-LIF set-up.

The intensity levels in the images captured by the camera are a function of depth [2], and the images can be easily converted to produce the instantaneous film heights from each image to give spatial and temporal evolution of the flow. The images were further analyzed to detect the size and location of the bubbles which show up by dark regions with a strong ring surrounding. The simple steps of the analysis were;

- Quantizing the image to limit the effect of noise on the results.
- Using a watershed to identify local minima.
- Filtering the detected minima to only detect true bubbles.

Each image was processed to produce the location and size of each bubble. These were collected to produce bubble size distributions for each image in further analysis.

3 Results

An example of a segment of one of the images ($V_g = 25\ ms^{-1}, Re_L = 220$) taken at two time steps; the first just before the droplet impact, the second 3.5 ms after the impact is shown in Figure 2. This clearly shows the bubbles created by the impact of the droplet. It is also possible to see secondary droplets these are not dark in the middle) that were also generated by the impact. The slow moving ripples in the film can also be seen to move downstream in the period of time between the images. The capillary wave ripple from the impact of the droplet is clearly seen in the left of the second picture.

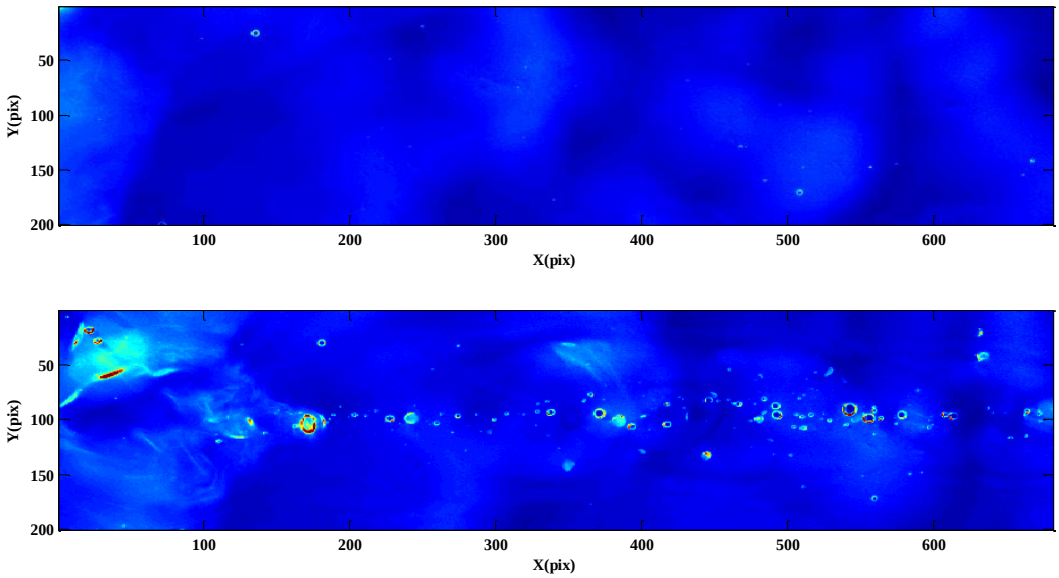

Figure 2: The top image shows the film heights in the moments before the impact of a droplet. The bottom image shows the stream of bubbles generated by the impact of the droplet.

The effect of the gas and liquid flow rate on the size distribution of the bubbles for all 9 cases is show in Figure 3. The legend was considered unimportant since the distributions are similar within the uncertainty when normalized against the number of bubbles in each flow condition. This is surprising. What is also clear is that similar to [6], there are two regions to the distribution. The transition between the two occurs about at a bubble radius of 80 microns at the highest velocity cases.

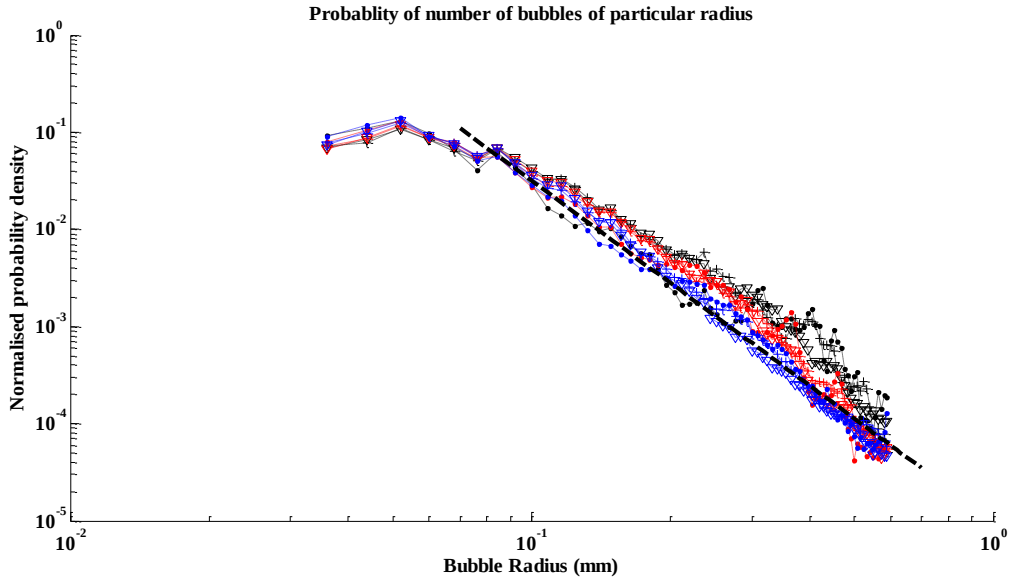

Figure 3: This shows the similarity in the distribution of bubble size for all 9 cases.

These averages are of a bi-modal system. The images either have disturbance waves or do not. The presence of disturbance waves can easily be identified by considering the sum of heights of the film in each image. This sum gives the total volume of fluid present at any time in the area under consideration. When there is a disturbance wave, this increases. The images can therefore be classified into images with a disturbance wave, and images without a disturbance wave. Phase averaging is difficult since these are irregular events, so a Proper orthogonal decomposition of the individual image distributions was carried out to identify if there were regular patterns that dominated the flow. This POD technique has been successfully used in other work to identify spatial and temporal modes that could potentially be linked to important physical mechanisms [8]. POD produces as many modes as there are images for each analysis, but in this case, 98% of the energy was contained in only the first two modes. This strongly suggests that this is a bimodal system with two states.
The zero order mode (which usually relates to the average) contained 95 % of the energy and the first order mode contained 3 % of the energy. Further modes are significantly smaller and so can be ignored.
The shape of the first two modes are similar for all cases (Figure 4) again suggesting that the physical mechanisms are the same for all 9 cases of Reynolds and gas velocity. To understand this in more detail, it is necessary to consider the temporal evolution of these modes.

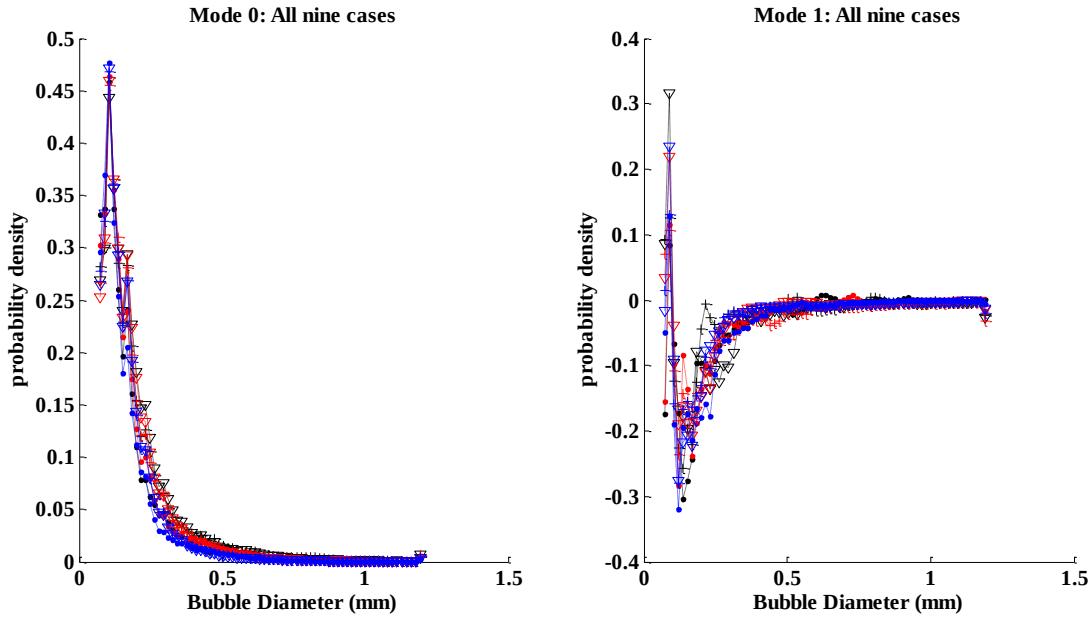

Figure 4: The left image shows that the zero-order mode of the POD analysis which contains about 95% of the energy is consistent across all 9 cases under investigation. The right hand image shows that this is also the case for the 1st order mode which contains about 3% of the energy.

The temporal coefficients of the first three modes are shown in Figure 5a. Figure 5b shows the relationship between the total volume of fluid present in each image compared to the number of bubbles. The three segments are stitched together here as seen by the sharp transitions. A comparison of the volume (which demonstrates when a disturbance wave is present) to the magnitude of the first mode of the distributions, has been compared to show that the first mode is directly proportional to the volume of fluid. The second mode has no correlation to the presence of the disturbance waves as do all the other modes, but the first mode does react to the presence of the wave. The effect of the first mode is to modify the shape of the zero order mode when the disturbance wave passes. The magnitude of the first mode is significantly less than the magnitude of the dominant mode. Since each mode is defined so the energy of each mode shape is unity, this suggests that the effect of the disturbance wave on the distribution is slight. This is confirmed in Figure 5c since the main effect of the disturbance wave is to slightly increase the probability of larger bubbles.

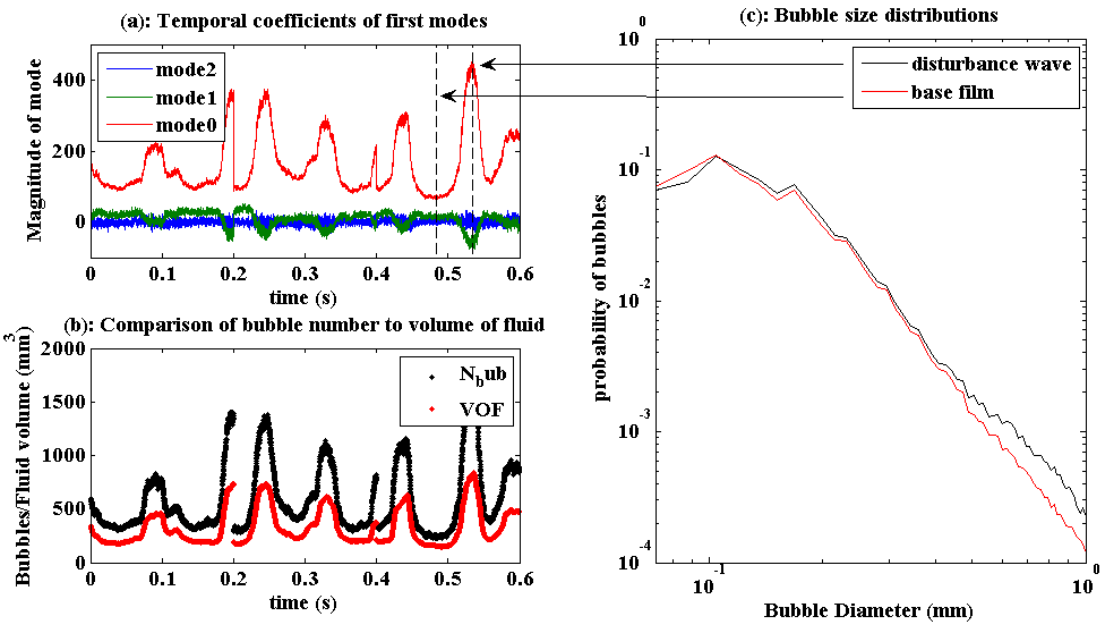

Figure 5: This figure relates the temporal coefficients of the POD analysis to the number of bubbles and presence of disturbance waves. (a) demonstrates that the zero order mode magnitude mimics the bubble numbers and volume of fluid present shown in (b). Figure (c) shows that the presence of the disturbance wave has only a minor effect on the overall bubble distribution.

As already discussed, the number of bubbles present in each image is linearly related to the total volume of fluid present in each image (Figure 6). However, the constant of proportionality (the bubble density) changes with both the gas flow rate and the liquid Reynolds number (Figure 7). The bubble density increases in a similar manner to the number of droplets entrained into the gas phase. This is not surprising since more entrained droplets mean more impacts of droplets and hence more bubble creation.

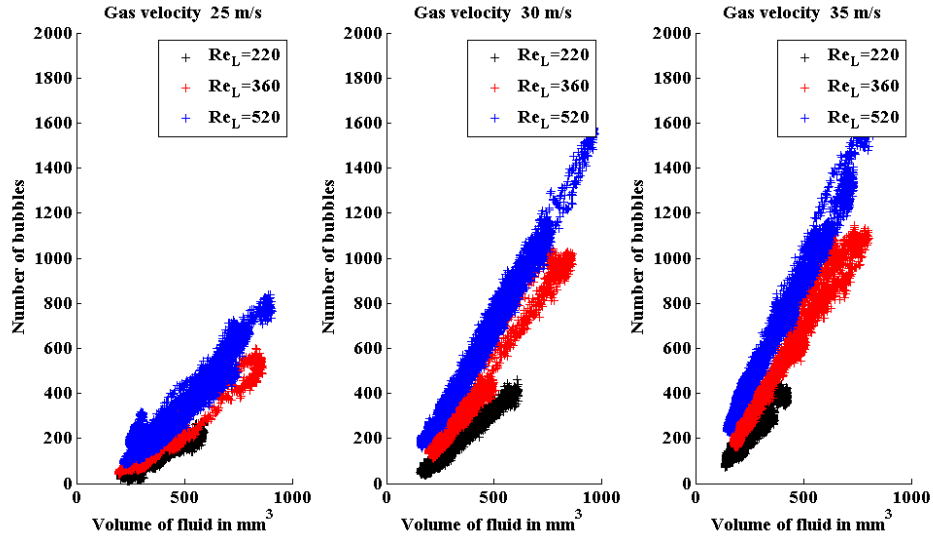

Figure 6: The linear relationship between the number of bubbles and the total volume of fluid present in each image is demonstrated in this figure. It is evident that the bubble density is a function of both the gas velocity and the Reynolds number of the liquid film.

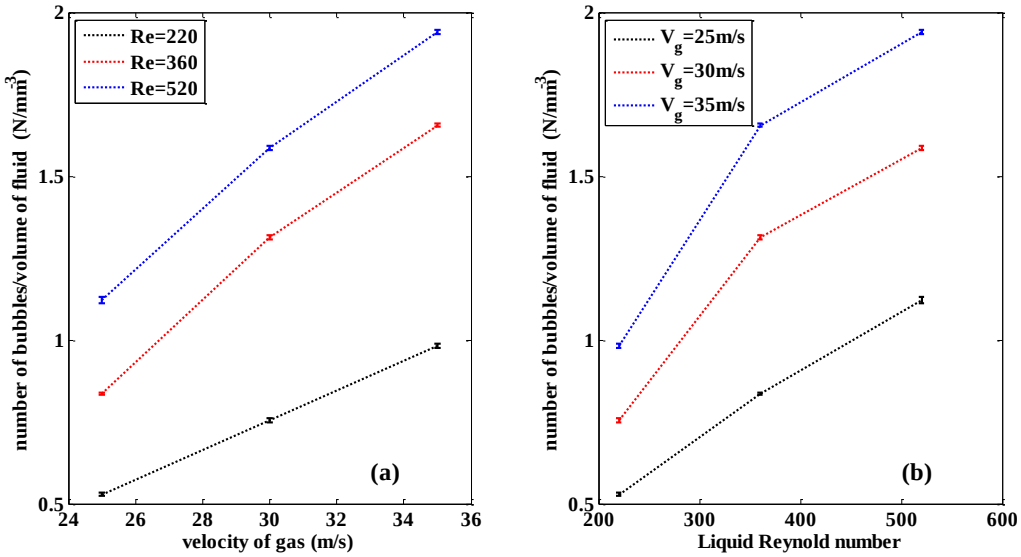

Figure 7: This figure shows that the bubble density increases with both velocity of the gas and liquid Reynolds number.

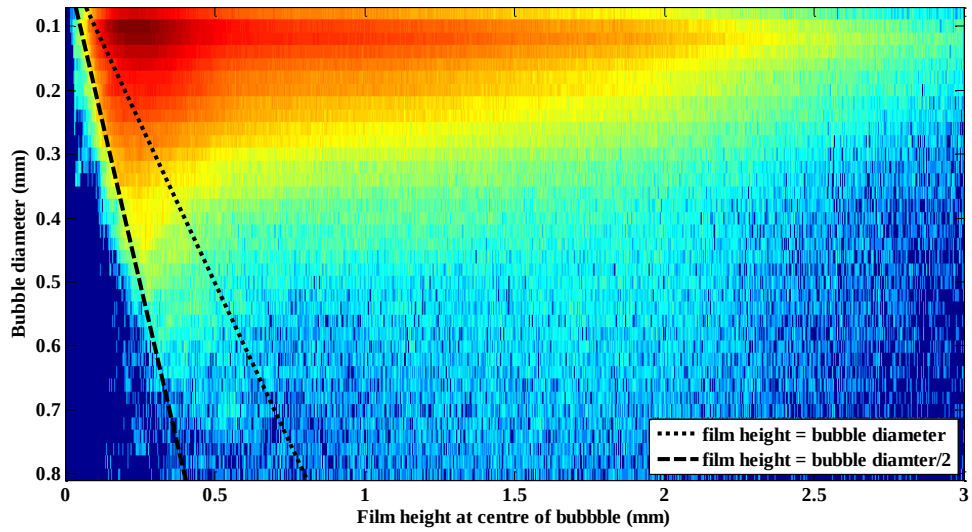

Figure 8: The size of the bubbles is compared to the thickness of the film in this figure. It is clear that there are no bubbles of diameter smaller than half the film thickness. The dotted line shows when the film thickness is the same as the bubble diameter. Thie colour denotes the logarithm of the number of bubbles at each condition.

The collection of images can further be analysed to see how the thickness of the film affects the size of the bubble. The images were processed to find the average local film height around the location of each bubble. The correlation between the local film height and the bubble diameter is shown in Figure 8. Further analysis not shown here has determined that the bubble size distribution for any particular film height is self-similar to the averaged film height. This rule is only broken at thin film height. It is clear that there is a region at small film height where the maximum bubble size is a function of the local film height. Surprisingly the dashed line shown in the image that most closely fits this relationship suggests that there are bubbles with twice the size of the film thickness. The dashed line demonstrates when the bubbles are of the same diameter as the film thickness. Obviously this needs further investigation, but there is an obvious conclusion. The bubble diameter is a 2D measurement and it is assumed that the bubble is spherical. The most obvious conclusion is that the bubbles detected in this region are not spherical and this seems to be correlated with two observations; Firstly, observation of the occurrence of these bubbles show that these occur in the base film between the disturbance waves; secondly, these bubbles have been seen to burst in a number of visualizations, which suggests that they are unstable. The presence of non-spherical bubbles has important ramifications in applying this work to heat transfer. These non-spherical bubbles will act as a barrier to heat

transfer from the gas to the wall or vice-versa and could affect the performance of steam heat exchangers for example.

4 Conclusions

In this paper the bubble density and distribution of size was investigated for sheared gas-liquid flow in a rectangular duct. The BB-LIF technique was demonstrated to give significant improvements in the spatial and temporal information of the flow with spatial resolutions of 0.040 mm and temporal resolutions of 0.1 ms. The results show that the majority of the bubbles created are by the re-entrainment of droplets sheared from the ripples on the disturbance waves. There appears to be some correlation between the density of bubbles entrained and the number of droplets sheared with a clear increase with both Reynolds number of film and velocity of the gas.

Acknowledgements. The work was supported by UK EPSRC Program Grant MEMPHIS (EP/K003976/1). Authors are grateful to the Roll-Royce UTC (University of Nottingham) for access to the flow facility.

References

[1] D. E. Woodmansee and T. J. Hanratty, "Mechanism for the removal of droplets from a liquid surface by parallel air flow," *Chemical Engineering Science,* vol. 24, pp. 299-307, 1969.

[2] A. V. Cherdantsev, , D. B. Hann and B. J. Azzopardi, "Study of gas-sheared liquid film in horizontal rectangular duct using high-speed LIF technique: Three-dimensional wavy structure and its relation to liquid entrainment," *International Journal of Multiphase Flow,* vol. 67, pp. 52-64, 2014.

[3] S. V. Alekseenko, V. A. Antipin, A. V. Cherdantsev, S. M. Kharlamov and D. M. Markovich, "Investigation of waves interaction in annular gas-liquid flow using high-speed fluorescent visualisation technique," *Microgravity Science and Technology,* vol. 20, pp. 271-275, 2008.

[4] D. J. Rodrigues and T. A. Shedd, "Entrainment of gas in the liquid film of horizontal, annular, two phase flow.," *International Journal of Mulit-phase flow,* vol. 30, no. 6, pp. 565-583, 2004.

[5] S. Alghoul, C. N. Eastwick and D. B. Hann, "Droplet impact on shear-driven liquid films," *Atomisation and sprays,* vol. 21, no. 833-846, 2011.

[6] G. B. Deane and M. D. Stokes, "Scale dependence of bubble creation mechnisms in breaking waves," *Nature,* vol. 418, pp. 839-844, 2002.

[7] A. V. Cherdantsev, D. B. Hann, B. N. Hewakandamby and B. J. Azzopardi, "STUDY OF DEPOSITION OF DROPLETS FROM THE GAS CORE ONTO A GAS-SHEARED LIQUID FILM," in *13th ASian symposium on Visualisation*, Novosibirsk, Russia, 2015.

[8] G. Berkooz, P. Holmes and J. L. Lumley, "The Proper Orthogonal decomposition in the analysis of turbulent flows," *Annual Review of Fluid Mechanics,* vol. 25, pp. 539-575, 1993.